A simulation system based on mixed-hybrid finite elements for thermal oxidation in semiconductor technology

Paola Causin

INRIA Rocquencourt
Domaine de Voluceau, Rocquencourt BP 105
78153 Le Chesnay Cedex, France

Marco Restelli, Riccardo Sacco *

MOX - Modeling and Scientific Computing
Dipartimento di Matematica "F. Brioschi"
Politecnico di Milano, via Bonardi 9, 20133 Milano, Italy

Abstract

In this work we deal with the numerical simulation of thermal oxidation in silicon device technology. This application involves the coupled solution of a diffusion-reaction problem and of a fluid-structure interaction problem. These two problems are mutually dependent through the exchange of stresses and fluxes that are typically post-processed fields in standard finite element approaches, and as such they may suffer from a lack of accuracy and from physical inconsistencies. In this article, we propose a novel approach to the simulation of the thermal oxidation process, that is characterized by the use of mixed and hybrid finite elements. The main advantage of such formulations is that stresses and fluxes are directly computed quantities, rather than obtained from post-processing techniques. We also address the procedures and the techniques that must be devised for handling the coupled interaction problem and the presence of a computational grid moving in time. The numerical approach we propose is eventually validated on a realistic example of the thermal oxidation process in a local oxidation structure (LOCOS).

Key words: thermal oxidation, semiconductor technology, dual mixed formulations, primal hybrid formulations, dual hybrid formulations.

---

* Corresponding author:
Email address: riccardo.sacco@mate.polimi.it (Riccardo Sacco).
URL: http://mox.polimi.it (Riccardo Sacco).

Preprint submitted to Elsevier Science *16 April 2003*

1 Introduction and motivation

The up-to-date technology in silicon integrated circuits involves the continuous embedding, butting and overlying of structural elements. Such elements, characterized by strongly heterogeneous mechanical properties, develop during fabrication stresses that can produce defects leading to current leakages and short-circuits that affect the electrical performance of the device. Therefore, *process device simulation* based on accurate physical models and advanced numerical methods can provide an important tool to drive the design strategy.

In this article, we concentrate on one of the several steps involved in device manufacturing, namely the thermal oxidation process, which tipically occurs in the isolation of adjacent electrically active zones on a semiconductor chip and in the fabrication of Metal Oxide Semiconductors devices (MOS).

The first satisfactory mathematical model for the thermal oxidation process was proposed in [11], where a one-dimensional diffusion-reaction equation provided an approximation of the physical phenomenon. Several corrections have been then proposed in order to accomplish for a more detailed analysis, for example in the case of thin oxide films [17]. More advanced models including the influence of the stress field on the oxide growth have then been developed in [20] guided by the experimental works of [5]. In particular, the fluid-mechanical description of silicon dioxide has gone from a purely elastic approach [16] to linear viscous [9] and nonlinear viscous models, even adopting highly sophisticated models as done in [21].

The numerical solution of the problem has been pursued mainly using finite element methods, as done in the code SUPREM [13] and its subsequent versions, and in the code NOVEL [18]. In these codes, standard finite element formulations are generally adopted. In this paper we exploit instead the use of mixed and hybrid finite element formulations. Since the two subproblems involved in thermal oxidation (oxygen diffusion and consequent silicon dioxide volumetric expansion) are mutually dependent through the exchange of stresses and fluxes, these latter quantities need be very accurately represented. This latter is indeed the main goal of mixed-hybrid formulations, where stresses and fluxes are *directly computed quantities*, rather than obtained from post-processing techniques.

The paper is organized as follows. We start giving in Sect.2 a brief overview of the physical aspects underlying the oxidation process and its overall mathematical modeling. In Sect.3 we discuss the mathematical model for the oxidant diffusion-reaction process and its numerical approximation by a primal hybrid finite element method implemented as a nonconforming approach (see [22,24]). In Sect.4 we discuss the mathematical model for stress generation in the struc-

ture and its numerical approximation using the dual-mixed hybrid (DMH) finite element method introduced and analyzed in [8]. Sect.5 deals with the algorithm used to iteratively solve the problem, and in particular with the part concerning the fluid-mechanical analysis. Due to the presence of a moving boundary, special techniques are required to manage the mesh in order to preserve its quality during process simulation. These techniques are described in Sect.6. In Sect.7 we show the numerical results obtained in the simulation of a real-life semiconductor device, and we collect in the concluding Sect. 8 some remarks and possible improvements on the oxidation process simulation.

2 Physical and mathematical modeling of thermal oxidation

In this section we give a brief description of the thermal oxidation process and provide some details about its mathematical modeling (for a more comprehensive discussion of the mathematical models of the thermal oxidation process, we refer to [20] and [21]).

The oxidation process consists in growing at high temperature a layer of silicon dioxide (SiO_2) on a silicon wafer bulk (Si). The Si surface is partially masked by a silicon-nitride (Si_3N_4) pattern impermeable to the oxidant penetration and is exposed to oxygen or water vapor at high temperature for a certain oxidation time (generally, 1-2 hours). The oxygen diffuses through the oxide and reacts with the silicon at the Si-SiO_2 interface. Since the SiO_2 has a molar volume 2.2 times larger than Si, at each time of the process a volume fraction of the new grown oxide replaces the silicon that has been consumed, while the remaining volume fraction pushes the old oxide upward. This constrained volume expansion gives rise to large stresses and in particular causes the SiO_2 to undergo a compressive state and the Si to undergo a tensile state. Experimental evidence [20,5] shows that this state of stress significantly affects both the O_2 diffusion in the pre-existing SiO_2 layer and also the chemical reaction kinetics between the O_2 and the Si. The combination of these effects alters the final shape of the Si-SiO_2 system that presents non planar regions (even when the oxide grows on planar regions) and gives rise to the so-called "bird's beak" region. A schematic representation of the thermal oxidation process in a local oxidation structure is shown in Fig.1.

The mathematical model of the process is constituted by a sequence of quasi-stationary steps each involving the solution of two PDE systems over a domain whose shape is changing in time. The first system is a diffusion-reaction problem for the oxidant and the second system is a stress analysis problem in the oxide, nitride and silicon bulk. The two PDE systems are mutually dependent: the diffusion and kinetic reaction coefficients as well as the geometry of the deformed domain depend on the stress distribution; in turn, the chemical reac-

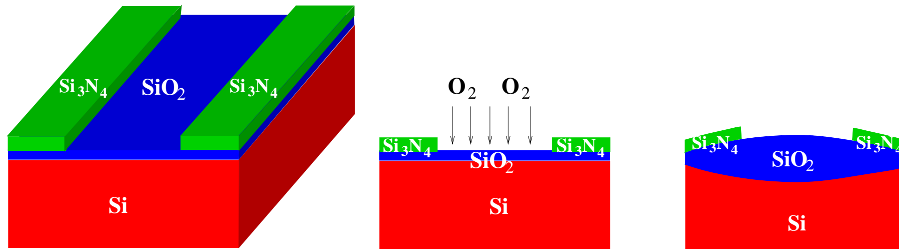

Fig. 1. Schematics of the thermal oxidation process in a local oxidation structure: 3D model (left), 2D reduction (center) at the beginning of the oxidation and 2D model (right) after process completion.

tion forces the oxide-silicon interface to move, driving the mechanical problem. After solving the diffusion-reaction problem, a stress analysis is performed to compute the new stress field and the resulting deformed configuration of the structure (see Fig.2). In particular, the stress analysis phase introduces a second nested level of coupling, since it requires solving a set of coupled mechanical problems, each one in a different material. In the present work, the Si_3N_4 mask and the Si bulk are modeled as linear elastic materials, while a non-Newtonian incompressible fluid model with nonlinear stress-dependent viscosity is used for the SiO_2 [20]. It appears evident that the data exchanged between the sub-blocks in both the coupled systems are fluxes and stress dependent quantities, so that the quality of their approximation clearly affects the accuracy of the overall computation.

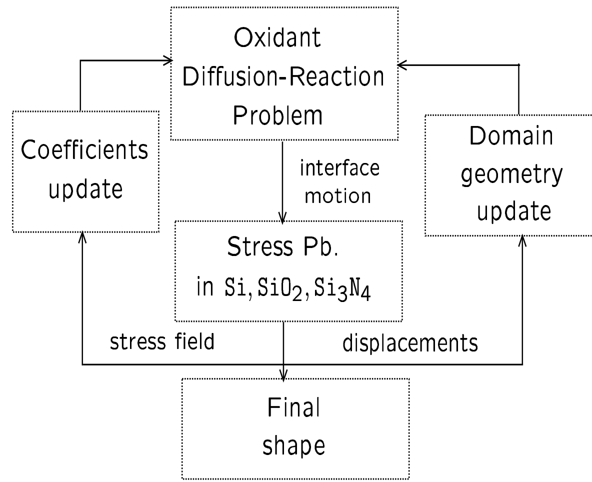

Fig. 2. Flow chart of the thermal oxidation process simulation.

3 Diffusion-Reaction Problem

The process of oxidant diffusion in the SiO_2 domain is described by an elliptic boundary value problem (Fick's law) driven by the O_2 ambient concentration

and by the chemical reaction between the O_2 and the Si species occurring at the SiO_2-Si interface (see Fig.3). The oxidation diffusion in nitride and silicon is negligible if compared with the diffusion in the oxide domain. For this reason, the diffusion problem is solved only in this latter region. Moreover, since the timescale for oxygen diffusion in the oxide is much smaller than the timescale governing the movement of the interface, the thermal oxidation problem can be treated using a *quasi-stationary* approximation, *i.e.*, at each time step a stationary problem for diffusion (and displacement) can be solved.

The diffusion-reaction problem reads:
find the oxidant concentration C in the oxide domain Ω such that

$$\begin{cases} -\mathrm{div}\,(D\nabla C) = 0 & \text{in} \quad \Omega \\ C = C^* & \text{on} \quad \Gamma_D, \\ D\dfrac{\partial C}{\partial n} + k_s C = 0 & \text{on} \quad \Gamma_R, \\ D\dfrac{\partial C}{\partial n} = 0 & \text{on} \quad \Gamma_N, \end{cases} \tag{1}$$

where on the domain boundary $\Gamma = \Gamma_D \cup \Gamma_N \cup \Gamma_R$ with outward unit normal vector n, we prescribe the ambient O_2 concentration C^* (on Γ_D), we include the effects of the chemical reaction (on the Si-SiO_2 interface Γ_R), D being the diffusion coefficient and k_s being the reaction coefficient, and we prescribe no-flux boundary conditions (on Γ_N) in correspondence of the metal stripe and of the vertical symmetry axis. The diffusion and reaction coefficients are defined as the following functions of the stress field [20]

$$D = D_0 \exp\left(\frac{pV_d}{K_B T}\right), \qquad k_s = k_{s_0} \exp\left(\frac{\sigma_{nn} V_r}{K_B T}\right), \tag{2}$$

where $\sigma_{nn} := (\sigma\, n) \cdot n$, p is the hydrostatic pressure, K_B is the Boltzmann constant, T is the process temperature, D_0 and k_{s_0} are the stress-free diffusion and reaction coefficients and V_d and V_r are suitable activation volumes. A schematic representation of problem (1) with its boundary conditions is shown in Fig.3. Notice that, due to symmetry with respect to the central vertical axis, only one half of the domain of Fig.1 is considered.

The new oxide formed at the interface with the silicon defines at each step the position of the interface itself. To express the velocity of propagation of the interface discontinuity, we introduce the variable $p_{ox} = D\nabla C$ representing the oxidant flux. This latter quantity and the interface normal velocity are related by the following Rankine-Hugoniot condition (see [21])

$$\int_{\Gamma_R} [\![\, p_{ox} \cdot n \,]\!]\, ds - \int_{\Gamma_R} [\![\, C \,]\!] V_n\, ds = 0 \quad \text{on } \Gamma_R, \tag{3}$$

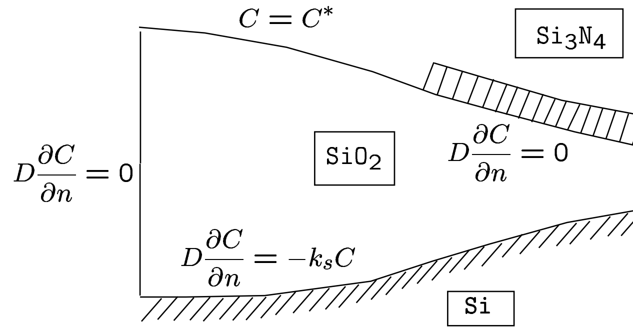

Fig. 3. Computational domain and boundary conditions for the diffusion-reaction problem.

where the symbol $[\![\cdot]\!]$ indicates the jump of the quantity across the interface Γ_R (that represents a line of discontinuity), V_n is the normal velocity of the interface (the unit normal vector being oriented from the oxide to the silicon). Relation (3) can be satisfied by enforcing the following (stronger) pointwise condition

$$V_n = \frac{[\![p_{ox} \cdot n]\!]}{[\![C]\!]} \qquad \text{on } \Gamma_R. \tag{4}$$

3.1 Finite Element Discretization

In view of the finite element approximation of (1), we introduce a regular partition $\mathcal{T}_h$ of Ω (see [10]) into triangles K such that $\overline{\Omega} = \bigcup_{K\in\mathcal{T}_h} \overline{K}$ and we indicate by $\partial\mathcal{T}_h$ the set of the edges of $\mathcal{T}_h$. For each element $K \in \mathcal{T}_h$, we denote by $|K|$ and h_K the area and the diameter of K, respectively, while for each edge $E \in \partial\mathcal{T}_h$ we denote by h_E the length of E. We also denote by ∂K the boundary of K and by n_K the unit outward normal vector along the boundary ∂K and for each node N_p of $\mathcal{T}_h$, we denote by $\mathcal{P}_p$ the patch of elements which have N_p as a common vertex. Finally, we denote by $\mathbb{P}_r(K)$, $r \geq 0$, the space of polynomials of degree $\leq r$ on each element K.

The diffusion-reaction problem (1) is solved using a primal hybrid method implemented as a nonconforming method, that reads:

find $C_h^{NC} \in W_{h,C^*}^{NC}$ such that

$$\sum_{K\in\mathcal{T}_h} \left(\int_K D\nabla C_h^{NC} \cdot \nabla v_h \, dx + \int_{\partial K\cap\Gamma_R} D^{-1} k_s \, C_h^{NC} \, v_h \, ds \right) = 0 \qquad \forall v_h \in W_{h,0}^{NC} \tag{5}$$

where for any given function $g_D : \Gamma_D \to \mathbb{R}$ we define W_{h,g_D}^{NC} as the set of functions that are:

- affine on each $K \in \mathcal{T}_h$;
- continuous at the midpoint of each internal edge of $\partial\mathcal{T}_h$ and attain at the midpoint of each edge lying on the Dirichlet boundary Γ_D the value of the average of g_D on that edge.

We refer to [22,24,4] for a comprehensive mathematical presentation of the primal hybrid/nonconforming formulation. Here, we only observe that the nonconforming approximation is more flexible (*i.e.*, less stiff) than the standard piecewise linear continuous finite element approximation. Moreover, the fluxes represented as independent variables enjoy the property of local auto-equilibrium and satisfy interelement traction reciprocity (see [4], Ch.1).

In the primal hybrid method, the approximate concentration C_h is a piecewise linear *discontinuous* function over $\mathcal{T}_h$ and the approximate fluxes $p_{ox,h} \cdot n$ are piecewise constant over $\partial\mathcal{T}_h$. The degrees of freedom for C_h and $p_{ox,h} \cdot n$ are shown in Fig. 4 (left).

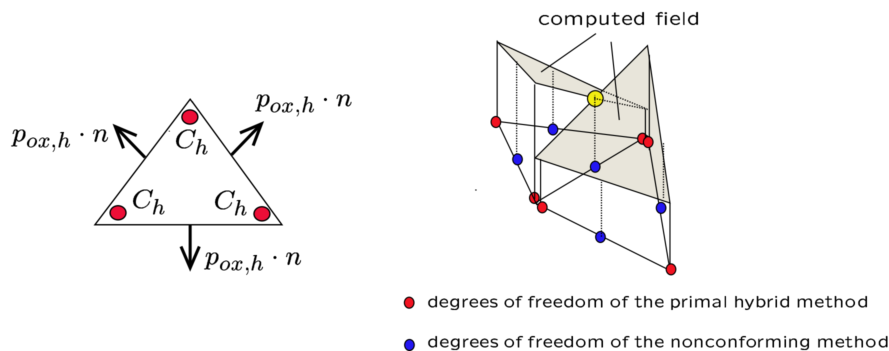

Fig. 4. Degrees of freedom for C_h and $p_{ox,h} \cdot n$ for the primal hybrid formulation (left) and coincidence with the nonconforming approximation (right).

The nonconforming approach is the most efficient way for coding a primal hybrid method, since after elimination of the variable $p_{ox,h} \cdot n$, it leads to a symmetric positive definite algebraic system of dimension equal to the sum of the number of internal edges and the number of edges belonging to Γ_N. This latter system can be regarded as a *generalized displacement problem* for the variable C_h^{NC} which is readily verified to *coincide* with the variable C_h computed by the primal hybrid formulation (see Fig. 4, right). The flux $p_{ox,h} \cdot n$ can be recovered by a post-processing procedure. In our case, this procedure can be conveniently limited to the elements having an edge on Γ_R, *i.e.* where the oxidant flux is needed to compute the interface velocity using (4).

4 Fluid-mechanical problem

Several possibilities exist for the mechanical modeling of the materials involved in oxidation process; in particular, different continuum-mechanics models need be adopted to describe faithfully the mechanical behavior of each material (oxide, silicon and nitride). In accordance with the experimental results of [5,20], the Si_3N_4 stripe and the Si bulk can be modeled - in a first basic implementation - as linear elastic materials (with anisotropic elastic properties in the case of Si), while it is apparent that a non-Newtonian model is needed for the SiO_2. Precisely, the SiO_2 can be represented by an incompressible fluid with nonlinear viscosity of Eyring type

$$\mu(\sigma) = \mu_0 \frac{\tau_{max}/\sigma_c}{\sinh(\tau_{max}/\sigma_c)}, \qquad \tau_{max} = \sqrt{(\sigma_{11} - \sigma_{22})^2/4 + \sigma_{12}^2}, \qquad (6)$$

where μ_0 is the stress-free constant viscosity and $\sigma_c = 2K_B T/V_c$, is a critical stress value, V_c being an activation volume.

In this work we adopt for the discretization of the fluid-mechanical problem the dual mixed-hybrid finite element formulation (DMH) proposed and analyzed in [8]. The DMH formulation is a mixed formulation capable of dealing with both compressible and incompressible regimes, as happens in the case at hand. This avoids introducing the quasi-incompressible approximation for handling the incompressible fluid problem or the difficulty of using - and maintaining - two separate computer codes, which is the commonly adopted procedure when compressible and incompressible problems coexist within the same physical model.

4.1 Formulation of the continuum-mechanics problem

In this section, we illustrate the mixed form of the linear isotropic elasticity model problem that will serve as the basic setting for the DMH formulation. The extension of the method to deal with anisotropic linear elastic materials is carried out in [6], while the treatment of the elasticity model problem in the incompressible case with nonlinear viscosity (Stokes problem for a non-Newtonian fluid) is deferred to Sect.5.

Let $M^{2\times 2} = \{\tau \in \mathbb{R}^{2\times 2}\}$, and $M^{2\times 2}_{skew} = \{\tau \in M^{2\times 2} : \tau + \tau^T = 0\}$. Then, the mixed formulation of the linear elasticity problem reads: Given a volume force $f : \Omega \to \mathbb{R}^2$, a displacement $u_D : \Gamma_D \to \mathbb{R}^2$, a traction $g_N : \Gamma_N \to \mathbb{R}^2$, find a displacement $u : \Omega \to \mathbb{R}^2$, a stress $\sigma : \Omega \to M^{2\times 2}$, a pressure parameter

$p : \Omega \to \mathbb{R}$ and a rotation tensor $\gamma : \Omega \to M^{2\times 2}_{skew}$, such that

$$\begin{cases} -\mathrm{div}\,\sigma = f & \text{in } \Omega \\ \sigma = 2\mu_{mat}(\nabla u - \gamma) - \mu_{mat}\rho\, p\, \delta & \text{in } \Omega \\ p = -\dfrac{1}{2}\,\mathrm{tr}\,\sigma & \text{in } \Omega \\ \mathrm{as}\,\sigma = 0 & \text{in } \Omega \\ u = u_D & \text{on } \Gamma_D \\ \sigma\, n = g_N & \text{on } \Gamma_N, \end{cases} \tag{7}$$

where $\mathrm{tr}\,\sigma = \sum_{i=1}^{2} \sigma_{ii}$, $\mathrm{as}\,\sigma = \sigma_{21} - \sigma_{12}$, δ is the 2×2 identity tensor and $\rho = \lambda_{mat}/(\mu_{mat}(\lambda_{mat} + \mu_{mat}))$, λ_{mat}, μ_{mat} being the Lamé coefficients of the material such that $\lambda_{mat} = +\infty$ for an incompressible material, with $\rho = 1/\mu_{mat}$ in the incompressible case. The variable γ is the infinitesimal rotation tensor that allows to weaken the symmetry constraint on σ and was introduced in the PEERS formulation [1]. The variable p is a *pressure parameter* that allows for a straightforward discrete treatment of the incompressible case ($\lambda_{mat} = +\infty$) and is the main novelty of the present formulation with respect to the original PEERS approach. For $\lambda_{mat} \to +\infty$, system (7) can be indeed conveniently interpreted as the conservative form of the Stokes equations in fluid dynamics

$$\begin{cases} -\mathrm{div}\,\sigma = f & \text{in } \Omega \\ \sigma = 2\nu\epsilon(u) - p\delta & \text{in } \Omega \\ \mathrm{div}\, u = 0 & \text{in } \Omega \\ u = u_D & \text{on } \Gamma_D \\ \sigma\, n = g_N & \text{on } \Gamma_N, \end{cases} \tag{8}$$

where $\epsilon(u) = (\nabla u + (\nabla u)^T)/2$ is the strain rate tensor, $\nu = \mu_{mat}$ is the kinematic viscosity and u is to be intended here as a velocity field. Indeed, using in $(7)_2$ the fact that $\varepsilon(u) = \nabla u - \gamma$, taking the trace of this latter relation, and using the definition $(7)_3$ of p, we get

$$\mathrm{tr}\,\epsilon(u) = \mathrm{div}\, u = \frac{1}{2\mu_{mat}}(\mathrm{tr}\,\sigma + 2\mu_{mat}\rho\, p) = \frac{p}{\mu_{mat}}(\mu_{mat}\rho - 1),$$

that for $\lambda_{mat} = +\infty$ recovers the incompressibility constraint $\mathrm{div}\, u = 0$.

System (7) is the starting point for introducing the DMH formulation addressed in the next sections. The distinct feature of formulation (7) is that it incorporates the idea of the introduction of the pressure variable originally proposed in the works [14,15] into the stress-displacement mixed approach with a

relaxed symmetry of the stress tensor. For an alternative stress-displacement unified mixed formulation in the isotropic case, we refer to [12].

4.2 Finite element approximation

The linear elasticity problem (7) is numerically solved using the dual-mixed hybrid (DMH) method proposed, analyzed and extensively validated in [8,6]. In order to introduce the discrete DMH formulation we define for every $K \in \mathcal{T}_h$, the following finite element spaces:

$$\Sigma_{g_N,h} = \left\{ \tau_h^K \in (\mathbb{RT}_0(K) \oplus \mathcal{B}_K)^2 \; \forall K \in \mathcal{T}_h, \; \tau_h n = g_N \text{ on } \Gamma_N \right\},$$

$$U_h = \left\{ v_h^K \in (\mathbb{P}_0(K))^2 \; \forall K \in \mathcal{T}_h \right\}, \quad \Lambda_h = \left\{ \mu_h \in (R_0(\partial K))^2 \; \forall K \in \mathcal{T}_h \right\},$$

$$W_h = \left\{ \theta_h \in C^0(\overline{\Omega}) \mid \theta_h^K \in (\mathbb{P}_1(K))^4 \; \forall K \in \mathcal{T}_h \right\}, \quad Q_h = \left\{ q_h^K \in \mathbb{P}_0(K) \; \forall K \in \mathcal{T}_h \right\},$$

where $\mathbb{RT}_0(K)$ is the Raviart Thomas finite element space of lowest order [23], $R_0(\partial K)$ is the space of piecewise constant functions on each edge of ∂K and $\mathcal{B}_K = \text{curl}(b_K) = (\partial b_K/\partial y, -\partial b_K/\partial x)^T$, b_K being the cubic bubble function on K. The DMH approximation of the continuum mechanics problem reads: find $(\sigma_h, u_h, \lambda_h, \gamma_h, p_h) \in \Sigma_{g_N,h} \times U_h \times \Lambda_h \times W_h \times Q_h$ such that

$$\begin{cases} a(\sigma_h;\tau_h) + b(u_h,\lambda_h,\gamma_h,p_h;\tau_h) = G(\tau_h) & \forall \; \tau_h \in \Sigma_{0,h}, \\ b(\sigma_h;v_h,\mu_h,\theta_h,q_h) + c(p_h;q_h) = F(v_h) & \forall \; (v_h,\mu_h,\theta_h,q_h) \in U_h \times \Lambda_h \times W_h \times Q_h. \end{cases} \tag{9}$$

where

$$a(\sigma_h;\tau_h) = \frac{1}{2\mu_{mat}} \int_\Omega \sigma_h : \tau_h \, dx \qquad \forall \sigma_h \in \Sigma_{g_N,h}, \quad \forall \tau_h \in \Sigma_{0,h},$$

$$b(v_h,\mu_h,\theta_h,q_h;\tau_h) = \sum_{K \in \mathcal{T}_h} \left(\int_K v_h \cdot \text{div}\, \tau_h \, dx - \int_{\partial K} \mu_h \cdot (\tau_h \, n) \, ds \right)$$
$$+ \int_\Omega \frac{\rho}{2} q_h \, \text{tr}\,(\tau_h) \, dx + \int_\Omega \theta \, \text{as}(\tau_h) \, dx \quad \forall (v_h,\mu_h,\theta_h,q_h) \in U_h \times \Lambda_h \times W_h \times Q_h, \; \tau_h \in \Sigma_0,$$

$$c(p_h;q_h) = \int_\Omega \rho \, p_h \, q_h \, dx \qquad \forall p_h, q_h \in Q_h,$$

$$G(\tau_h) = \int_{\Gamma_D} u_D \cdot \tau_h \, n \, ds \qquad \forall \tau \in \Sigma_0, \qquad F(v_h) = \int_\Omega f \cdot v_h \, dx \qquad \forall v_h \in U_h.$$

The additional unknown λ_h in (9) is the Lagrangian multiplier that enforces the condition of traction reciprocity of the stress σ across each edge of $\mathcal{T}_h$. Relaxing the traction reciprocity constraint turns out to be advantageous in the numerical implementation of the DMH formulation since it allows to perform static condensation of the discontinuous variables σ_h and u_h, leading to a linear algebraic system of reduced size whose unknowns are the interface displacements λ_h (hybrid variables) and the pressure and rotational parameters p_h and γ_h. This latter system can be regarded as a *generalized displacement-pressure-rotation* formulation of the linear elasticity (Stokes) problem. The degrees of freedom for the various unknowns in the DMH finite element approximation are shown in Fig. 5.

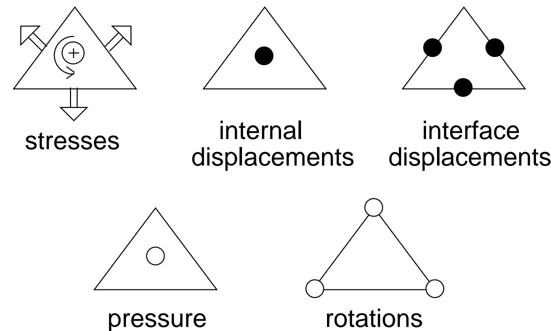

Fig. 5. Degrees of freedom in the DMH finite element method.

5 Treatment of the coupled problem

This section deals with the description of the algorithm for the simulation of the time evolution of the thermal oxidation process. A preliminary discussion of this subject has been already carried out in Sect. 2 where a flow-chart illustrates the procedure. Here in Sect. 5.1 we set up more in detail the sequence of steps to be executed at each time level of the simulation algorithm, while in Sect. 5.2 we give some details on the proper modeling of silicon-to-oxide volumetric expansion. Then, the solution approach to the fluid-mechanical problem is addressed in Sect. 5.3 and Sect. 5.4.

5.1 Algorithm for the simulation of the thermal oxidation problem

At each time level, the simulation procedure of the thermal oxidation process consists in executing the following steps until a fixed oxidation time T_{ox} is reached:

(1) solving a diffusion-reaction problem for the oxidant within the SiO_2 domain (cf. Sect. 3), in order to determine the oxidant concentration at the SiO_2-Si interface Γ_{int};
(2) computing the velocity V_n normal to Γ_{int} by (4);
(3) repositioning the mesh nodes belonging to Γ_{int} according to the value V_n;
(4) determining the portion of the Si domain that is crossed by Γ_{int} during the time interval (such a portion corresponds to the amount of Si volume that is involved in the oxidation reaction);
(5) solving, through a coupled algorithm, the fluid-mechanical problem in all the materials (cf. Sect. 4);
(6) repositioning the mesh nodes according to the computed displacement/velocity field;
(7) relaxing the computational grid according to the quality control criteria described in Sect. 6.

5.2 Modeling the volumetric expansion

Silicon volumetric expansion occurs during oxidation due to the fact that the molar volume of SiO_2 is larger than the molar volume of Si. To account for this phenomenon, two modeling approaches can be pursued. The first approach consists in enforcing a *discontinuity* in the normal component of the velocity field at the interface. By doing so, volume expansion is included in the model through a boundary condition imposed on the two elastic and fluid subproblems [20,13]. In the present work we adopt a second approach, that is analogous to that proposed in [21], consisting in the introduction of a *stress-free deformation associated with the oxidation reaction.* By doing so, the velocity field remains a continuous function at the interface. This latter approach appears to be more attractive compared to the previous one in view of the introduction of a viscoelastic description of oxide rheology.

We assume that in the silicon dioxide domain the following decomposition of the strain rate tensor $D_v = (\nabla v + (\nabla v)^T)/2$ holds

$$D_v = D_\Delta + D_\sigma, \tag{10}$$

D_Δ being the stress-free deformation rate and D_σ being the strain rate associated with the state of stress in the material. Assuming that $\mathrm{tr}\, D_\sigma = 0$ (i.e. no volumetric deformation is associated with the stress state), we have

$$\mathrm{tr}\ D_v = \frac{1}{V_\Omega}\frac{dV_\Omega}{dt} = \mathrm{tr}\, D_\Delta, \tag{11}$$

V_Ω and dV_Ω being the specific volume of the silicon dioxide undergoing the volumetric expansion and its variation due to the chemical reaction, respectively. Having introduced the decomposition (10), the stress-strain constitutive

equation for a fluid in which a stress-free expansion is occurring reads

$$\frac{1}{2\mu_{mat}}\sigma + \frac{1}{2\mu_{mat}}p\delta - D_v = -D_\triangle. \tag{12}$$

Relation (12) differs from the usual law valid for a Newtonian fluid due to the presence of the (known) term $D_\triangle$, that can be straightforwardly accomodated within the DMH formulation discussed in Sect. 4. In order to correctly account for the increase of the silicon molar volume $V_{\mathtt{Si}}$ to the oxide molar volume $V_{\mathtt{SiO_2}}$ according to the ratio $V_{\mathtt{SiO_2}}/V_{\mathtt{Si}} = 2.2 \equiv \gamma_{ox}$, the stress-free deformation rate $D_\triangle$ must obey the following relation

$$\int_{t^n}^{t^{n+1}} \mathrm{tr}\, D_\triangle \, dt = \int_{V_{\mathtt{Si}}}^{V_{\mathtt{SiO_2}}} \frac{dV_\Omega}{V_\Omega} = \log(\gamma_{ox}).$$

5.3 Stability analysis of decoupled algorithms for fluid-structure interaction in thermal oxidation

In this section, we present two possible decoupled algorithms for handling the fluid-structure interaction in the thermal oxidation process. For both methods, a stability analysis is carried out with reference to a one-dimensional fluid-structure interaction model problem. Despite the simplicity of the model, the results of the stability analysis indicate the impossibility to apply decoupled algorithms to the problem at hand, this being a strong motivation toward the introduction of some coupling mechanism between the fluid and mechanical subproblems. With this aim, two basic strategies can be devised, the first strategy being the use of relaxation schemes (in the framework of domain-decomposition techniques, see [19]), the second strategy being the use of a fully coupled solution of the fluid-structure problem. In this article, we have pursued this latter alternative, as discussed and motivated in Sect. 5.4, deferring the former alternative, that is clearly attractive from the point of view of computational efficiency, to future investigation.

In view of the presentation of the iterative algorithms, we refer ourselves to the simple one-dimensional fluid-structure interaction model problem constituted by an elastic element with stiffness k placed in series with a viscous damper with viscosity r (see Fig.6). We also suppose to neglect inertial terms, as is the case of the thermal oxidation process.

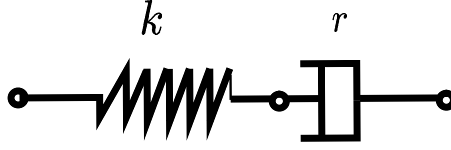

Fig. 6. Spring-damper model.

We assume throughout that the two endpoints of the system are kept fixed and denote by u the displacement of the midpoint of the system. Moreover, let $F_k = -ku$ be the force on the spring and $F_r = -r\dot{u}$ be the force on the damper. Then, the following equation describes the time evolution of the spring-damper system

$$r\dot{u} + ku = 0. \tag{13}$$

To solve (13), the following two iterative algorithms, denoted by (A) and (B), may be employed. Algorithm (A) is described by the relations:
given $u^n, n \geq 0$, compute the sequence

$$F_k^n = -ku^n, \quad v^{n+1/2} = -\frac{F_r^n}{r} = \frac{F_k^n}{r}, \quad u^{n+1} = u^n + v^{n+1/2}\Delta t, \tag{14}$$

where u^n is the displacement at the time level t^n and $v^{n+1/2}$ is the velocity which leads to the displacement u^{n+1} of time level t^{n+1} starting from u^n. Algorithm (A) can be interpreted as a Dirichlet (for the structure)-Neumann (for the fluid) iteration. Solving (14) for u^n we get

$$u^n = C\lambda^n, \qquad \lambda = 1 - \frac{k\Delta t}{r}, \tag{15}$$

C being a constant depending on the initial condition. The sequence u^n remains bounded as $n \to \infty$ if

$$|\lambda| < 1 \qquad \Longrightarrow \qquad \Delta t < 2\,\frac{r}{k}. \tag{16}$$

Condition (16) states that algorithm (A) is stable provided that the time step is *lower* than a fixed threshold value.

Algorithm (B) is described by the relations:
given u^{n-1}, u^n, $n \geq 1$, compute the sequence

$$v^{n+1/2} = \frac{u^n - u^{n-1}}{\Delta t}, \quad F_r^{n+1} = -rv^{n+1/2}, \quad F_k^{n+1} = -ku^{n+1} = -F_r^{n+1}. \tag{17}$$

Algorithm (B) can be interpreted as a Neumann (for the structure)-Dirichlet

(for the fluid) iteration. Solving (17) for u^n we get

$$u^n = C_1 \lambda_1^n + C_2 \lambda_2^n, \qquad \lambda_{1,2} = \frac{1}{2}\frac{r}{k\Delta t}\Big(\pm \sqrt{1 + 4\frac{k\Delta t}{r}} - 1 \Big) \tag{18}$$

C_1 and C_2 being constants depending on the initial condition. The sequence u^n remains bounded as $n \to \infty$ if

$$|\lambda_{1,2}| < 1 \qquad \Longrightarrow \qquad \Delta t > 2\,\frac{r}{k}. \tag{19}$$

Condition (19) states that algorithm (B) is stable provided that the time step is *larger* than a fixed threshold value.

In the case of the fluid-structure interaction problem in thermal oxidation, it turns out that the coupling $\texttt{SiO}_2$-$\texttt{Si}_3\texttt{N}_4$ should be treated by a scheme of type (A), while the coupling $\texttt{Si}$-$\texttt{SiO}_2$ should be treated by a scheme of type (B). To see this point, suppose to advance from t^n to t^{n+1} according to the following decoupled strategy:

- computation of the velocity and stress field in the oxide subdomain. This problem is governed by the forcing terms due to volumetric expansion through the following interface boundary conditions: at the $\texttt{Si}$-$\texttt{SiO}_2$ interface Dirichlet boundary conditions are imposed based on the displacement computed in the silicon subdomain at time t^n, while at the $\texttt{SiO}_2$-$\texttt{Si}_3\texttt{N}_4$ interface Neumann boundary conditions are imposed based on the stress field computed in the nitride subdomain at time t^n;
- computation of the displacement and stress field in the silicon and nitride subdomains. These two problems are governed by the following interface boundary conditions: at the $\texttt{Si}$-$\texttt{SiO}_2$ interface Neumann boundary conditions are imposed based on the stress field computed in the oxide subdomain at the present time level, while at the $\texttt{SiO}_2$-$\texttt{Si}_3\texttt{N}_4$ interface Dirichlet boundary conditions are imposed by integration of the velocity computed in the oxide subdomain at the present time level.

According to the above strategy, it clearly follows that the $\texttt{SiO}_2$-$\texttt{Si}_3\texttt{N}_4$ coupling is treated by a scheme of type (A) since the elastic material imposes a force and the viscous material imposes a displacement, while the $\texttt{Si}$-$\texttt{SiO}_2$ coupling is treated by a scheme of type (B) since the elastic material imposes a velocity to the boundary of the fluid subdomain whose response is in turn represented by a system of loads on the elastic material. Coming back to the stability conditions (16) and (19), we see that they require to take $\Delta t < 2\frac{r_{\texttt{SiO}_2}}{k_{\texttt{Si}_3\texttt{N}_4}}$ and $\Delta t > 2\frac{r_{\texttt{SiO}_2}}{k_{\texttt{Si}}}$ in the case of algorithm (A) and (B), respectively. These two requirements are mutually conflicting, as the typical values of the physical parameters in the problem at hand do not allow to pick up a value of Δt satisfying the above conditions *simultaneously*. For this reason, the use of

the (computationally attractive) decoupled algorithms has been abandoned in favor of the coupled approach described in the forthcoming section.

5.4 A coupled algorithm for fluid-structure interaction in thermal oxidation

The difficulties described in the previous section can be overcome by solving the fluid-mechanical problem in thermal oxidation through a coupled approach. This strategy appears to be particularly well suited for the DMH formulation since this latter is able to cope automatically (due to the unified framework discussed in Sect. 4.1) with materials exhibiting heterogeneous compressibility properties by properly employing the formal analogy existing between the incompressible elasticity equations and the Stokes problem in fluid dynamics.

Let us thus consider the fluid-mechanical system defined in the spatial domain $\Omega = \Omega_{el} \cup \Omega_{fl}$, Ω_{el} being the region exhibiting elastic behavior (Si and Si_3N_4) and Ω_{fl} being the region with fluid behavior (SiO_2). Let $\Gamma_i = \partial\Omega_{el} \cap \partial\Omega_{fl}$ denote the interface separating the two regions. Since we are interested in the quasi-stationary evolution of the system, we have $\Omega_{el} = \Omega_{el}(t)$ and $\Omega_{fl} = \Omega_{fl}(t)$, and the same assumption holds for the source term f and the boundary conditions. The mathematical model of the fluid-structure interaction problem reads:

$$\left\{ \begin{array}{l} \left\{ \begin{array}{lll} \operatorname{div}\sigma^{el} + f^{el}(t) = 0 & \text{in} & \Omega_{el}(t), \\ A\sigma^{el} - \varepsilon^{el} = 0 & \text{in} & \Omega_{el}(t) \end{array} \right. \\ \left\{ \begin{array}{lll} \operatorname{div}\sigma^{fl} + f^{fl}(t) = 0 & \text{in} & \Omega_{fl}(t), \\ \dfrac{1}{2\mu_{mat}}\sigma^{fl} + \dfrac{1}{2\mu_{mat}}p\delta - D_v = -D_\Delta & \text{in} & \Omega_{fl}(t), \\ \operatorname{div} v = 0 & \text{in} & \Omega_{fl}(t) \end{array} \right. \\ \left\{ \begin{array}{lll} \dot{u} = v & \text{on} & \Gamma_i(t), \\ \sigma^{el}n + \sigma^{fl}n = 0 & \text{on} & \Gamma_i(t), \end{array} \right. \end{array} \right. \qquad (20)$$

where u and v denote the displacement and velocity field in the solid and in the fluid, respectively, f^{el} and f^{fl} are volume forces in the solid and in the fluid (equal to zero in the specific case of thermal oxidation), $\dot{u} = Du/Dt$ and A denote the material (or Lagrangian) velocity and the compliance tensor in the solid, respectively, $\varepsilon^{el}(u)$ is the strain tensor, and $D_v(v)$ and D_Δ are the complete strain rate tensor and the stress free strain rate tensor (see Sect.5.2), respectively. System (20) must be supplied with suitable Dirichlet and Neu-

mann boundary conditions on $\partial\Omega$. The interface conditions $(20)_6$ and $(20)_7$ enforce the continuity of the displacement (adherence condition) and the continuity of the normal stress (action and reaction principle), respectively. The approximation of $(20)_{1-2}$ and $(20)_{3-5}$ can be carried out by using separately in each material subdomain the DMH formulation. This requires to:

- discretizing in Ω_{el} stress, pressure, displacement and infinitesimal rotation fields;
- discretizing in Ω_{fl} stress, pressure, velocity and rotational velocity fields.

To close the problem, the interface conditions $(20)_6$ and $(20)_7$ must be added, after suitable discretization.

Within the context of dual-mixed hybrid formulations, treating condition $(20)_7$ turns out to be quite natural, since this condition amounts to enforcing the continuity of the normal stress across interelement edges. Having characterized the mathematical setting for the stress behavior at the interface, the discretization of $(20)_7$ follows the standard hybridization procedure based on the introduction of a Lagrange multiplier λ which is approximated by piecewise constant functions on each edge of Γ_i (cf. Sect. 4.2).

Treating the adherence condition $(20)_6$ is a more delicate question since it involves computing the time material derivative of the displacement of a point belonging to the interface. Notice that working under the hypothesis of small displacements for the solid region and neglecting the inertial terms, system (20) actually represents a lagrangian description for the structure, while the fluid is described under an eulerian framework.

In the following, we shall thus provide some considerations that justify the procedure for the computation of the above derivative that has been adopted in this work. With this aim, we start introducing the initial configuration of the system, denoted by Ω^0. Then, we denote by X the coordinates of a material point in the configuration Ω^0 with respect to an absolute frame of reference, while x denotes the coordinates of a material point in the configuration Ω^t that is occupied by the system at time t with respect to the same frame of reference. Moreover, let Φ^t be the map representing the displacement field of the material which leads from the initial configuration to the configuration Ω^t

$$\Phi^t : \Omega^0 \rightarrow \Omega^t, \qquad x(t, X) = \Phi^t(X).$$

The regularity of motion requires that Φ^t is a continuous and invertible map. Let now $\mathcal{T}_0$ denote a regular triangulation [10] of Ω^0 such that $\overline{\Omega}^0 = \bigcup_{K \in \mathcal{T}_0} \overline{K}$. (This assumption implies that $\overline{\Omega}^0$ has no curvilinear boundaries). Moreover,

we also assume that $\mathcal{T}_0$ satisfies the following condition

$$\exists\, \mathcal{E}_h^{\Gamma_i^0} \subset \mathcal{E}_h, \quad \mathcal{E}_h^{\Gamma_i^0} \neq \{\emptyset\}, \quad \text{such that} \quad \Gamma_i^0 = \bigcup_{e_i \in \mathcal{E}_h^{\Gamma_i^0}} e_i. \tag{21}$$

This condition states that the interface Γ_i is constituted solely by edges of $\mathcal{T}_0^0$ and that Γ_i does not cross any element of $\mathcal{T}_0^0$. Let us now consider a suitable discretization $\Phi^{t,h}$ of the map Φ^t

$$\Phi^{t,h} : \Omega^0 \to \Omega^{t,h},$$

$\Omega^{t,h}$ being the approximation of the configuration Ω^t that is obtained by applying $\Phi^{t,h}$. Moreover, let $\mathcal{T}_t$ be a regular triangulation of $\Omega^{t,h}$ such that $\overline{\Omega}^{t,h} = \bigcup_{K \in \mathcal{T}_t} \overline{K}$. We also assume that $\mathcal{T}_t$ is the image of $\mathcal{T}_0$ through $\Phi^{t,h}$

$$\mathcal{T}_t = \Phi^{t,h}(\mathcal{T}_0). \tag{22}$$

We adopt for $\Phi^{t,h}$ the affine map obtained from the nodal displacements computed with the reconstruction procedure illustrated in Sect. 6.1.

Assuming for the moment that Γ_i^t is *always* constituted by the same material points, (21) and (22) imply

$$\exists \mathcal{E}_h^{\Gamma_i^t} \subset \mathcal{E}^t{}_h \quad \text{such that} \quad \Gamma_i^t = \bigcup_{e_i \in \mathcal{E}_h^{\Gamma_i^t}} e_i \quad \forall t \in [0, T_{ox}]. \tag{23}$$

Denoting by $\eta_u^t(x,t)$ the basis functions for the discrete velocity in the fluid domain at time t, we have

$$\eta_u^t(x,t) = \eta_u^0 \circ (\Phi^{t,h})^{-1} = \eta_u^0(X(x,t)), \qquad x \in \Omega^t.$$

Now, using the fact that $\left.\frac{\partial \eta^0}{\partial t}\right|_X = 0$ we can write

$$\frac{D\lambda_u}{Dt}(x,t) = \left.\frac{\partial \lambda_u}{\partial t}\right|_X (x,t) = \sum_i \dot{\alpha}_{\lambda_u,i}(t)\ \eta_{u,i}^t(x,t) \tag{24}$$

Since for the interface edges we have $\eta_{\lambda_u,i}^t = \eta_{\lambda_v,i}^t$, relation $(20)_6$ reads

$$\dot{\alpha}_{\lambda_u,i}(t) = \alpha_{\lambda_v,i}(t). \tag{25}$$

When the above procedure is applied to the simulation of thermal oxidation, relations (22) and (23) are compatible for points lying on the SiO_2-Si_3N_4 interface but not for points lying on the Si-SiO_2 interface. Indeed, due to the chemical reaction, condition (22) would imply the interface to possibly cross

the interior of the elements, thus preventing the fulfilment of (23) and requiring to handle elements that have partly elastic constitutive behavior and partly a fluid behavior. In order to avoid this latter situation, we have decided to satisfy condition (23) at the price of sacrifying to fulfil condition (22) at the generic time t. As a consequence, condition (24) has only an approximate validity, this approximation being as much accurate as the displacement field across the interface is uniform in the direction of V_n.

5.4.1 Time advancing scheme

The spatial discretization of problem (20) gives rise to solving a Differential Algebraic system of equations (DAE) constituted by the algebraic equations emanating from $(20)_{1-5,7}$ and by the differential equations emanating from $(20)_6$. The DAE system can be cast into the following matrix form

$$C \begin{bmatrix} \dot{y} \\ \dot{z} \end{bmatrix} = K \begin{bmatrix} y \\ z \end{bmatrix} + b, \qquad C = \begin{bmatrix} I & 0 \\ 0 & 0 \end{bmatrix}, \tag{26}$$

where b is a given vector, I is the identity matrix and K is the stiffness matrix which is a nonlinear function of the geometry configuration of the system and of the stress state in the material through (6). System (26) has been solved using the θ-method, with an inner fixed-point iteration to handle the nonlinearity of the problem arising from (6) (the small geometrical deformation of the computational domain during the time step being neglected in the linearization procedure). To support the validity of this latter approximation, notice that the order of magnitude of the stress in the SiO_2 film (1000 MPa) implies a variation of the viscosity of three orders of magnitude according to (6).

To improve the time accuracy of the above procedure, we have also investigated the use of higher-order time advancing schemes. To test the procedure, we have applied the fifth-order BDF method implemented in the `Matlab ode15s` solver (see [26]) to approximate the time evolution of the model fluid-structure interaction problem described in [7]. Fig. 7 compares the error curves for the θ-method and the BDF scheme as functions of the computing time. The results show the dramatic improvement in computational efficiency due to the use of the higher-order method.

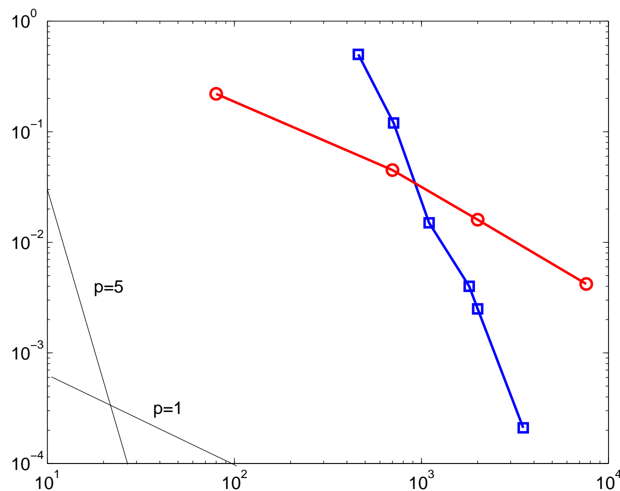

Fig. 7. Comparison between the θ-method (circles) and the BDF method (squares). On the x-axis the cpu time (in seconds) is reported, while on the y-axis the displacement error is reported.

We conclude this section by briefly discussing the quantitative choice of the time step during the simulation of the time evolution of the thermal oxidation process. On the one hand, a reasonable compromise must be reached between accuracy and total computational effort (consider that typical values of T_{ox} are of the order of 1 hour). On the other hand, since the incremental deformation of the device geometry is proportional to Δt, this latter quantity must be properly bounded in order to preserve an admissible geometry of the finite element mesh. Computational experience has shown that the need of maintaining a high quality of the grid, in particular during the starting phase of the process, can be satisfied by adopting the strategies described in Sect. 6 and taking a maximum value for Δt of the order of $20\,s$.

6 Grid management techniques

In this section we address the issue of the management of the computational grid. This aspect is crucial in the computer implementation of the algorithm described in Sect. 5.3 due to the need of maintaining a good quality of the mesh during the simulation of the thermal oxidation process evolution.

6.1 Reconstruction of the displacement field for grid updating

In order to update the mesh, we must dispose of the nodal displacement. Thus, given the *discontinuous* computed displacement field of our approximation, we

describe in this section the procedure for reconstructing a nodal-valued displacement field. The error analysis carried out in [8] shows that the interface displacement, denoted by λ_h, enjoys a higher convergence rate than the corresponding approximation of the displacement field inside each element, denoted by u_h. Then, the field λ_h is the preferable choice to reconstruct the displacement field. The problem is that λ_h is piecewise constant on *each edge* of the triangulation (cf. Sect. 4.2), whereas in order to deform the mesh we need dispose of singly defined nodal displacements. These latter must be thus reconstructed from the values λ_h, possibly *without substantial loss of accuracy* (or at least without spoiling the present order of convergence with respect of the mesh parameter h). To do this, we have developed an averaging procedure based on a mechanical analogy which assumes that each vertex of the mesh is connected to its neighbor through an elastic spring. Solving for the point of equilibrium of the system of springs subject to the given displacement λ_h yields the deformed configuration of the mesh (see Fig.8).

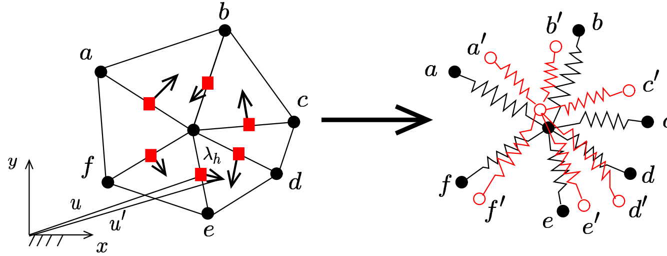

Fig. 8. The new position of the vertex is the point of equilibrium of the spring system subject to the displacements λ_h (red spring system).

In order to assess the quality of the results provided by the reconstruction procedure, a numerical experiment has been conducted on a test problem in the incompressible case (Stokes problem) for a fluid squeezed between two parallel plates moving one toward the other with constant velocity (see [8] for the details). In Fig.9 we represent as functions of the mesh discretization parameter h the maximum absolute errors between the exact solution u_{ex} and λ_h (computed at the midpoints of each edge) and between the exact solution and the reconstructed displacement u'_h (computed at the vertices of the mesh). We observe that the maximum error on the (reconstructed) vertex displacement field is larger than the maximum error on the edge midpoint displacement field. However, the $\mathcal{O}(h^2)$ convergence rate of the DMH formulation is maintained and the ratio between the two errors is acceptable. This behavior has been verified using both structured and unstructured meshes.

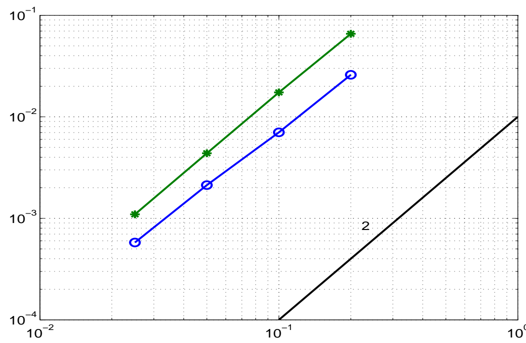

Fig. 9. Error quantities: $\max\limits_{p=1,\mathtt{NV}} |u_{ex,p} - u'_{h,p}|$,'*', and $\max\limits_{e=1,\mathtt{NEd}} |u_{ex,e} - \lambda_{h,e}|$,'o', where NV and NEd denote the number of vertices and edges of $\mathcal{T}_h$, respectively.

6.2 Preserving the mesh quality

During the simulation the quality of the grid tends to progressively deteriorate due to the advancing of the $\mathtt{Si}$-$\mathtt{SiO_2}$ interface and to the large displacements occurring in the oxide region (see Fig.10). To cope with the above problems,

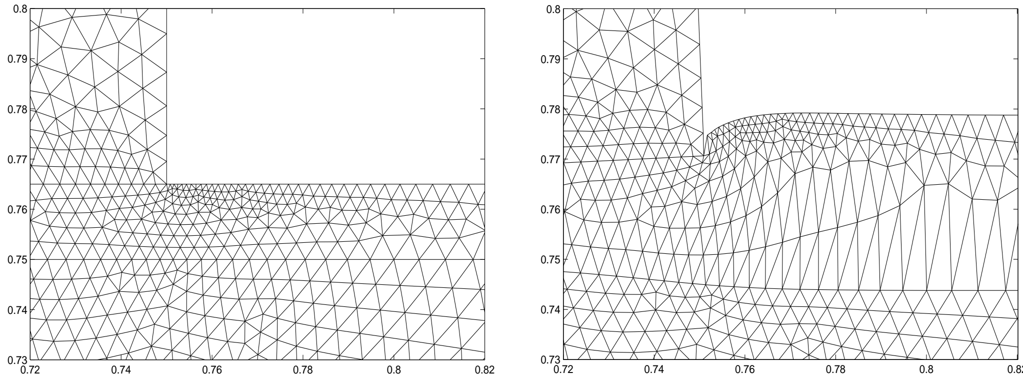

Fig. 10. Deformation of the grid during oxidation: starting grid (left) and deformed grid after 150 s (right).

after each step of the oxidation evolution a *regularization procedure* is applied to the current grid by suitably repositioning the mesh nodes without altering the topological structure of the grid itself. In order to drive the algorithm, we use a *quality index* defined for a mesh triangle K as (see [3])

$$\eta_K = 4\sqrt{3}\frac{|K|}{\sum\limits_{E\in\partial K} h_E^2}, \tag{27}$$

where $\eta_K = 1$ in the case of an equilateral triangle, while $\eta_K \to 0$ in the case of a degenerate element. Then, the regularization procedure consists in minimizing for each patch $\mathcal{P}_p$ surrounding the mesh node N_p the quantity $Q_p = \sum\limits_{K\in\mathcal{P}_p} 1/\eta_K$. Newton's method is used for solving numerically the mini-

mization problem, this not resulting into an appreciable overload with respect to the overall computational burden of the problem. The regularization technique based on the local control of the quality index (27) has been successfully implemented in the thermal oxidation simulation system discussed in the article, providing particular benefit in handling the case of *nonconvex* patches that frequently arise during deformation in the bird's beak region of the oxide (cf. Fig. 10 and Fig. 14). To improve the robustness of the procedure in particularly unfavorable situations (which is the present case as shown in Sect. 7), a *local remeshing* is performed whenever the quality index (27) falls below a fixed tolerance.

7 Numerical results

In this section we validate the performance of the coupled simulation algorithm described in Sect. 5 on a real-life thermal oxidation process test case. The geometry of the considered semiconductor domain is shown in Fig. 11 (left).

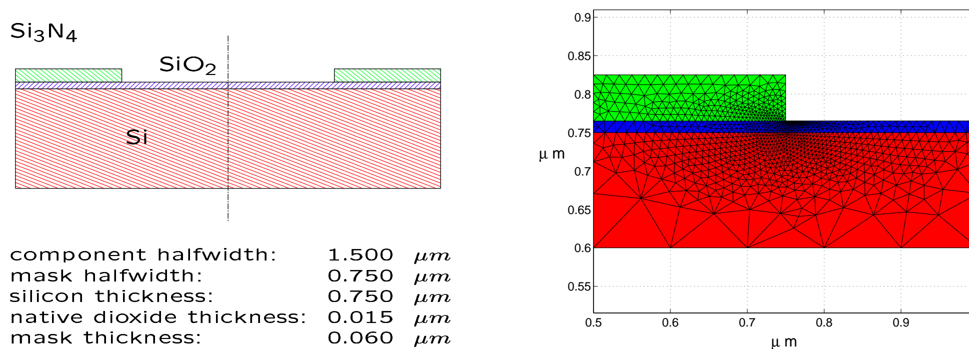

Fig. 11. The silicon wafer before oxidation (left): the green color denotes the $\mathtt{Si_3N_4}$ mask and the blue color denotes the native oxide film. The computational domain and its finite element discretization consisting of 2127 triangles (right).

The symmetry of the problem allows to limiting the simulation to half the region shown in Fig. 11 (left); The following values of the problem coefficients, relative to a wet oxidation, have been assumed in the numerical computations (see [11,20,2,25]):

diffusion-reaction problem:
$D_0 = 8 \times 10^{-2}\, \mu m^2\, s^{-1}$, $C_0 = 3 \times 10^7\, molecules\ \mu m^{-3}$, $V_d = 17 \times 10^{-6}\, \mu m^3$, $N_1 = 4.4 \times 10^{10}\, molecules\ \mu m^{-3}$, $k_{s,0} = 7.9 \times 10^{-1}\, \mu m\, s^{-1}$ and $V_r = 12.5 \times 10^{-6}\, \mu m^3$;

fluid-mechanical problem:
$E_{\mathtt{Si_3N_4}} = 0.39\, N\, \mu m^{-2}$, $\nu_{\mathtt{Si_3N_4}} = 0.3$, $\mu_{0,\mathtt{Si_3N_4}} = 20\, N\, s\, \mu m^{-2}$, $\sigma_{c,\mathtt{Si_3N_4}} = 0.1 \times$

$10^{-3}\,N\,\mu m^{-2}$, $c_{11,\mathtt{Si}} = 0.1657\,N\,\mu m^{-2}$, $c_{12,\mathtt{Si}} = 0.0639\,N\,\mu m^{-2}$ and $c_{44,\mathtt{Si}} = 0.0796\,N\,\mu m^{-2}$.
Notice that an orthotropic description of the elastic properties of the Si bulk has been assumed, due to the presence of different elastic coefficients $c_{ij,\mathtt{Si}}$. This issue requires to properly generalize the DMH formulation described in Sect. 4.1 to the case of a material governed by an anisotropic stress-strain relation (see [6,7]).

Plane strain conditions are assumed in the solution of the fluid-mechanical problem. A homogeneous Dirichlet boundary condition is enforced on the bottom of the domain, symmetry conditions hold on the vertical edges and a homogeneous Neumann condition is imposed on the remaining sides of the domain.

Figs. 12 and 13 show the computed results at the time levels $t_1 = 15\ s$ and $t_2 = 300\ s$. The various graphs include (ordered from left to right, top to bottom): the oxidant concentration, the σ_{xx}, σ_{yy} and σ_{yx} components of the stress tensor, the pressure distribution p and the maximum shear stress τ_{max}. This latter variable is of special relevance as it influences directly the value of the viscosity coefficient in the SiO_2 region.

The main production of a novel SiO_2 film occurs at the bird's beak region, where there is a large oxidant concentration at the Si-SiO_2 interface. Due to the volumetric expansion, the new oxide, constrained by the above Si_3N_4, results in a compressive state (negative values of σ_{yy}), and is forced to flow outward (a sort of horizontal outflow squeezing effect), this producing the characteristic "bird's beak"shape. On the contrary, we observe that only a small fraction of the available oxidant can diffuse throughout the interior region underneath the Si_3N_4 mask, where the SiO_2 production turns out to be negligible. This latter region, where the mask tends to be moved away from the oxide film, is thus characterized by a tensile stress state (positive values of σ_{yy}). As a consequence, the resulting load on the Si_3N_4 mask is a (counterclockwise) torque, balanced by the σ_{xx} distribution in the mask itself. During the oxidation process evolution, the stress field in the SiO_2 film tends to relax, due to the viscous flow, while the increased thickness of the film progressively inhibits further oxide production. As a consequence, the region characterized by a stress tensile state moves deeper under the Si_3N_4 mask. A more refined detail of the stress distribution in the bird's beak region of the device is shown in Fig. 14.

Turning to the quantitative analysis of simulation results, we observe that the computed stress exceeds the expected values, in particular as for the value of σ_{xx}, if compared to typical values in the literature (see [21,25]). An explanation to this effect is to be ascribed to the uncertainty in the values of the fluid-mechanical parameters of the various materials that are used in the numerical

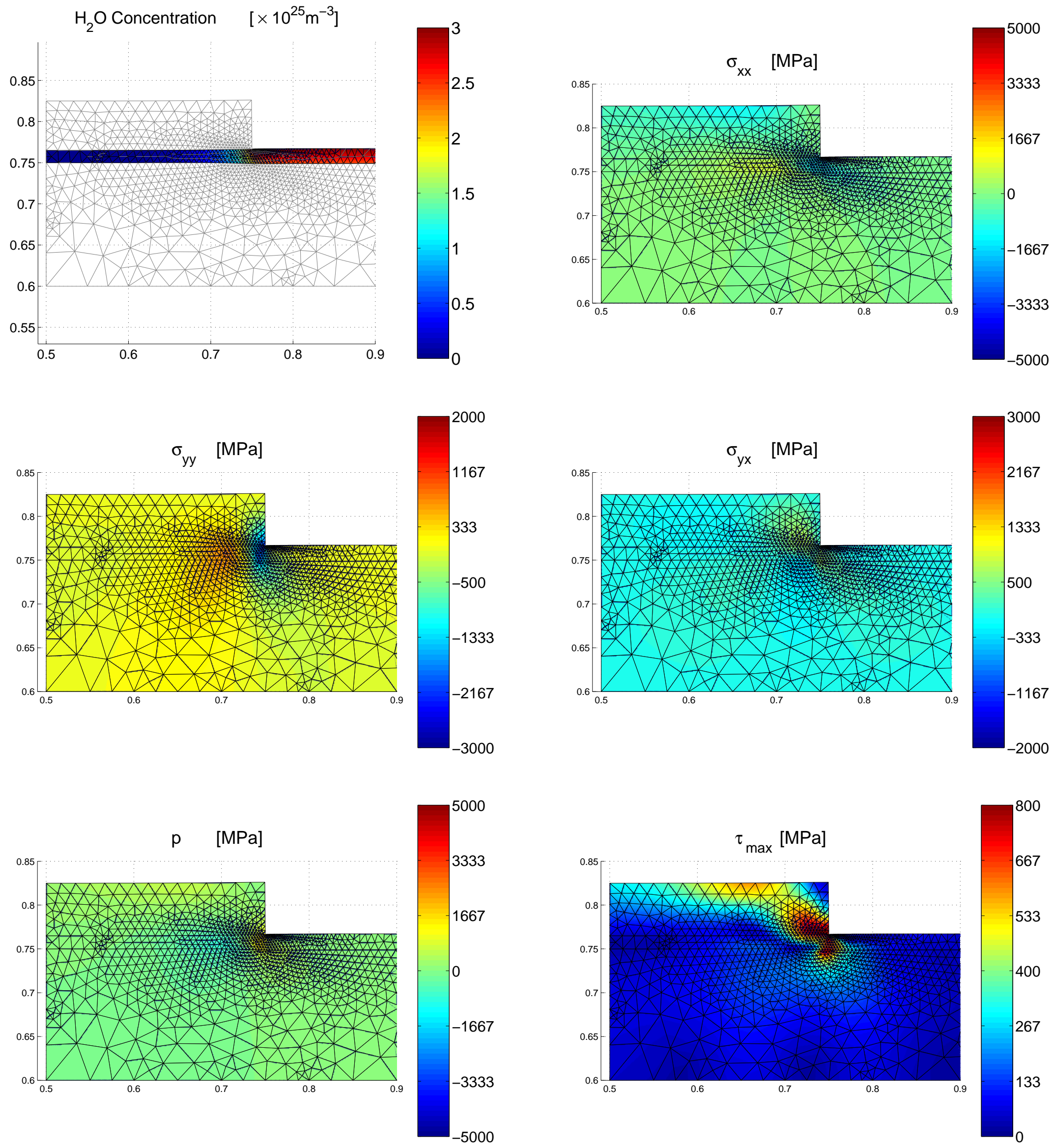

Fig. 12. Simulation results at $t_1 = 15\ s$.

simulation, in particular those relative to $\mathtt{SiO_2}$ and $\mathtt{Si_3N_4}$. Actually, while the elastic parameters for $\mathtt{Si}$ and the characteristic stress $\sigma_c = 100\ MPa$ for $\mathtt{SiO_2}$ are well established in the literature, no similar agreement seems to exist for the viscosity μ_0. As for $\mathtt{Si_3N_4}$, relatively few data are available and all of them are the result of the calibration between *viscoelastic* models and experimental data. The use of these parameters within a *linear elastic* model for $\mathtt{Si_3N_4}$ (as done in our simulation algorithm) can be clearly a source of inconsistency, due to the fact that the presently adopted model *does not* allow for stress relaxation during the oxidation process, and therefore it should be regarded as a first step toward a more extensive validation and improvement of the simulation algorithm.

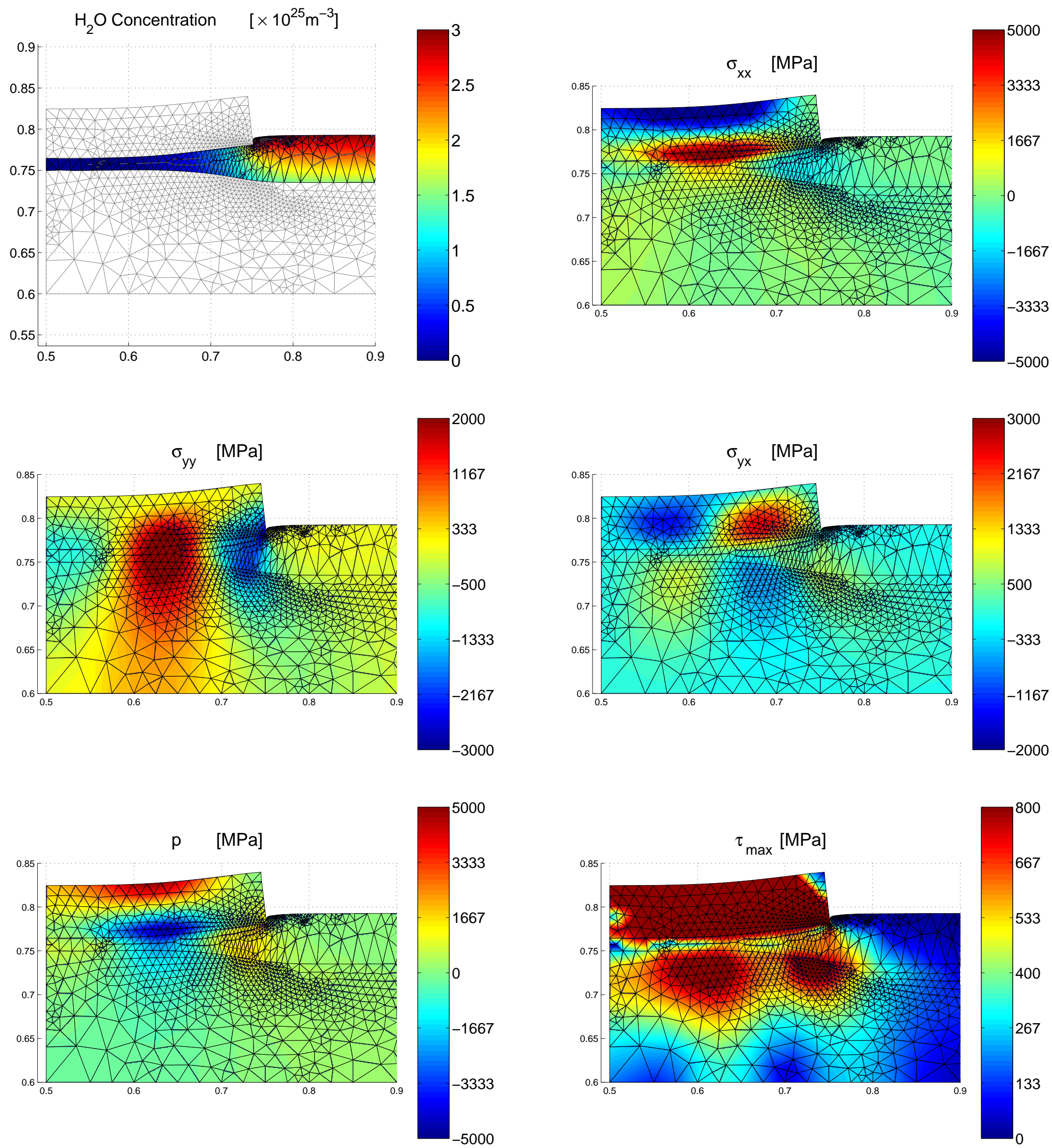

Fig. 13. Simulation results at $t_2 = 300\ s$.

8 Conclusions

In this work we have studied the numerical approximation of the thermal oxidation process in semiconductor technology using mixed-hybrid finite elements. The main goal of the research activity is twofold, on the one hand aiming to investigate and validate properties and potentialities of the above finite element methodologies, on the other hand willing to dispose of an accurate and flexible tool for the simulation of such a complex industrial-relevant problem.

The mathematical model of thermal oxidation requires solving a sequence

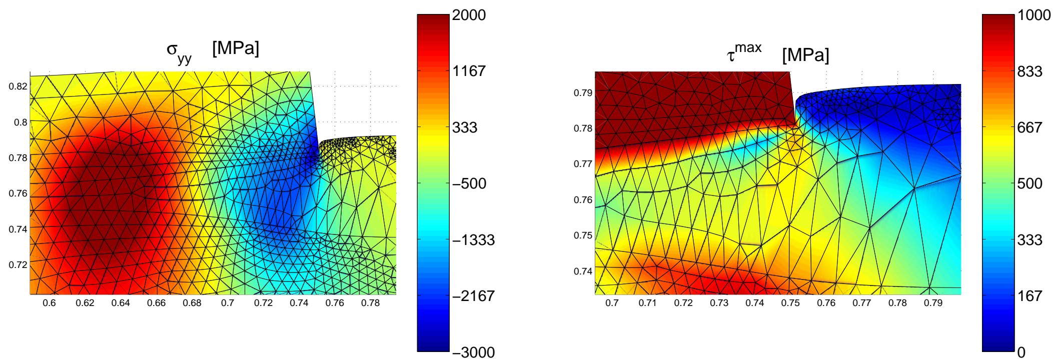

Fig. 14. Detailed view of the bird's beak region at $t_2 = 300\ s$.

of quasi-stationary systems of PDEs, namely, a diffusion-reaction problem for the oxidant and a fluid-mechanical problem in the three materials involved in the process, namely, Si (elastic anisotropic material), SiO_2 (viscous non-Newtonian fluid) and Si_3N_4 (elastic isotropic material). The diffusion-reaction problem is numerically solved using a primal-hybrid method implemented as a nonconforming generalized displacement formulation, while the fluid-mechanical problem is discretized using a dual-mixed hybrid formulation which is capable of treating in a unified and robust framework both compressible and incompressible regimes. Both formulations provide an accurate and self-equilibrated approximation of fluxes and stresses unlike standard displacement-based finite element approaches.

Special care is devoted to properly treating the fluid-structure interaction problem. In particular, a stability analysis reveals possible failure of decoupled algorithms, this prompting for the use of a coupled algorithm to handle the fluid-mechanical problem. With this aim, a θ-method is employed for advancing in time, while a fixed-point iteration is performed to account for the nonlinear dependence of the fluid viscosity on the shear stress in the oxide. The resulting scheme is robust and accurate, provided that suitable grid regularization techniques are adopted.

The numerical performance of the simulation tool are extensively validated on the solution of fluid-mechanical interaction model problems, as well as in the study of a real-life semiconductor oxidation problem. The obtained results exhibit in general good agreement with experimental data and the literature, although a better calibration of some problem coefficients is still needed to improve the quantitative adherence of the computed values of maximum stresses.

This latter issue is strictly connected with future research activity on both the model and the algorithm that have been considered in the present article. Among possible extensions, we mention:

- the introduction of a viscoelastic description of SiO_2 and Si_3N_4 rheology,

which allows to account for stress relaxation, and the adoption of an elasto-plastic constitutive law for `Si`;

- the improvement of the time-advancing strategy by resorting to the use of higher-order difference schemes;
- the adoption of relaxation schemes based on domain-decomposition techniques to improve computational efficiency in the solution of the fluid-structure interaction problem;
- the adoption of a suitable a posteriori error indicator to adaptively drive the grid management procedure;
- the extension of the simulation tool proposed in this article to deal with three-dimensional problems.

References

[1] D. Arnold, F. Brezzi, J. Douglas, Peers: A new mixed finite element for plane elasticity, Japan J. Appl. Math. 1 (1984) 347–367.

[2] R. Balboni, A. Armigliato and al., Tem/cbed determination of strain in silicon-based submicrometric electronic devices, Micron 31 (2000) 203–209.

[3] R. Bank, W. Coughran, W. Fichtner, D. Rose, R.K. Smith, Computational aspects of semiconductor device simulation, Process and Device Modeling (W.L. Engl, Ed.), North-Holland, Amsterdam (1986).

[4] F. Brezzi, M. Fortin, Mixed and Hybrid Finite Element Methods, Springer Verlag, New York, 1991.

[5] D. Cao, L. McWittie, W. Nix, K. Saraswat, Two-dimensional silicon oxidation: experiments and theory, IEDM Tech. Digest .

[6] P. Causin, Mixed-Hybrid Galerkin and Petrov-Galerkin Finite Element Formulations in Fluid Mechanics, Ph.D. thesis, Università degli Studi di Milano, `http://mox.polimi.it` (2002).

[7] P. Causin, R. Sacco, Mixed-hybrid Galerkin and Petrov-Galerkin finite element formulations in continuum mechanics, in: F. H.A. Mang, J. Eberhardsteiner (Eds.), Proceedings of the Fifth World Congress on Computational Mechanics (WCCM V), Vienna University of Technology, Austria, 2002, `http://wccm.tuwien.ac.at`.

[8] P. Causin, R. Sacco, A dual-mixed hybrid formulation for fluid mechanics problems: Mathematical analysis and application to semiconductor process technology, Comput. Methods Appl. Mech. Engrg. 192 (2003) 595–614.

[9] P. Chin, Two dimensional oxidation, PhD Thesis, Stanford University (1983).

[10] P. Ciarlet, The Finite Element Method for Elliptic Problems, North Holland, Amsterdam, 1978.

[11] B.E. Deal, A.S. Grove, General relationship for the thermal oxidation of silicon, J. Appl. Physics 36(12) (1965) 3370–3378.

[12] M. Farhloul, M. Fortin, Dual hybrid methods for the elasticity and the Stokes problems: a unified approach, Numer. Math. 76-4 (1997) 419–440.

[13] S.E. Hansen, M.D. Deal, SUPREM-IV.GS User's Reference Manual, Stanford University, 1994.

[14] L. Herrmann, Elasticity equations for incompressible and nearly - incompressible materials by a variational theorem, AIAA Jnl. 3-10 (1965) 1896–1900.

[15] L. Herrmann, R. Taylor, K. Pister, On a variational theorem for incompressible and nearly-incompressible orthotropic elasticity, Int. J. Solids Structures 4 (1968) 875–883.

[16] C.H. Hsueh, A.G. Evans, Oxidation induced stress and some effects on the behavior of oxide films, J. Appl. Physics 54(11) (1983).

[17] M. Navi, S.T. Dunham, Viscous compressible models for stress generation relaxation in SiO_2, J. of the Electrochemical Society 144(1) (1997) 367–371.

[18] J.P. Peng, D. Chidambarrao, G.R. Srinavasan, NOVEL. A nonlinear viscoelastic model for thermal oxidation of silicon, COMPEL, 10(4) (1991) 341–353.

[19] A. Quarteroni, A. Valli, Domain decomposition methods for partial differential equations, Clarendon Press, Oxford (1999).

[20] C. Rafferty, Stress effects in silicon oxidation - simulation and experiment, Ph.D. thesis, Stanford University (1990).

[21] V. Rao, T.J.R., Hughes, K. Garikipati, On modeling thermal oxidation in silicon part i-ii, Int. J. Num. Meth. Engr. 47 (2000) 341–377.

[22] P. Raviart, J. Thomas, Primal hybrid finite element methods for 2nd order elliptic equations, Math. Comp. 31-138 (1977) 391–413.

[23] P. Raviart, J. Thomas, A mixed finite element method for second order elliptic problems, in: I. Galligani, E. Magenes (Eds.), Mathematical Aspects of Finite Element Methods,I, Springer-Verlag, Berlin, 1977.

[24] J. Roberts, J. Thomas, Mixed and hybrid methods, in: P. Ciarlet, J. Lions (Eds.), Finite Element Methods, Part I, North-Holland, Amsterdam, 1991, vol.2.

[25] H. Rueda, Modeling of mechanical stress in silicon isolation technology and its influence on device characteristics, PhD thesis, University of Florida, 1999.

[26] L.F. Shampine, M.W. Reichelt, The Matlab ODE suite, SIAM J. Sci. Comput. 18 (1997) 1–22.